

Pixel-based correction for Charge Transfer Inefficiency in the *Hubble Space Telescope* Advanced Camera for Surveys

Richard Massey,^{1*} Chris Stoughton,² Alexie Leauthaud,³ Jason Rhodes,^{4,5}
Anton Koekemoer,⁶ Richard Ellis⁵ and Edgar Shaghouljian⁷

¹Royal Observatory, Blackford Hill, Edinburgh EH9 3HJ

²Fermi National Accelerator Laboratory, PO Box 500, Batavia, IL 60510, USA

³Physics Division, Lawrence Berkeley National Laboratory, Berkeley, CA 94720, USA

⁴Jet Propulsion Laboratory, California Institute of Technology, Pasadena, CA 91109, USA

⁵California Institute of Technology, 1200 East California Boulevard, Pasadena, CA 91125, USA

⁶Space Telescope Science Institute, 3700 San Martin Drive, Baltimore, MD 21218, USA

⁷Stanford University, Physics building, 382 Via Pueblo Mall, Stanford, CA 94305, USA

Accepted 2009 September 1. Received 2009 August 31; in original form 2009 August 5

ABSTRACT

Charge Transfer Inefficiency (CTI) due to radiation damage above the Earth's atmosphere creates spurious trailing in *Hubble Space Telescope* (*HST*) images. Radiation damage also creates unrelated warm pixels – but these happen to be perfect for measuring CTI. We model CTI in the Advanced Camera for Surveys (ACS)/Wide Field Channel and construct a physically motivated correction scheme. This operates on raw data, rather than secondary science products, by returning individual electrons to pixels from which they were unintentionally dragged during readout. We apply our correction to images from the *HST* Cosmic Evolution Survey (COSMOS), successfully reducing the CTI trails by a factor of ~ 30 everywhere in the CCD and at all flux levels. We quantify changes in galaxy photometry, astrometry and shape. The remarkable 97 per cent level of correction is more than sufficient to enable a (forthcoming) reanalysis of downstream science products and the collection of larger surveys.

Key words: instrumentation: detectors – methods: data analysis – space vehicles: instruments.

1 INTRODUCTION

Charge-Coupled Device (CCD) imaging detectors convert incident photons into electrons. The electrons are stored within a silicon substrate, in a pixellated grid of electrostatic potential wells that gradually fill up during an exposure. At the end of the exposure, the electrons are shuffled, row by row, to a readout register at the edge of the device. They are then counted and converted into a digital signal.

Above the Earth's atmosphere, a continuous bombardment of high-energy particles makes a harsh environment for sensitive electronic equipment. Protons, neutrons, high-energy electrons and heavy ions create bulk damage by colliding with and displacing atoms from the silicon lattice. The dislodged atoms can come to rest in the interstitial space, and the vacancies left behind move about the lattice until they combine with interstitial impurities, such as phosphorous, oxygen or another vacancy (Janesick et al. 2001). Such defects degrade a CCD's ability to shuffle electrons, known as its Charge Transfer Efficiency (CTE; Charge Transfer Inefficiency (CTI) = $1 - \text{CTE}$). Electrons can become temporarily trapped in the

local potential, then released after a delay that depends upon the properties of the lattice and impurities, and the operating temperature of the device (Shockley & Read 1952; Hall 1952). If a few electrons are trapped during CCD readout, and held while other electrons are moved along, they are released as a spurious trail (see Fig. 1). Regions of the image furthest from the readout register are worst affected, because electrons starting there encounter the most charge traps during their journey across the device.

CTI gets worse over time, as cumulative radiation damage creates more charge traps. By 2007 January, when the *Hubble Space Telescope* (*HST*) Advanced Camera for Surveys (ACS) encountered an electronic failure, the instrument had been in operation on-orbit for almost 5 years, and its Scientific Imaging Technologies (SITe) ST002A CCDs were already significantly affected by CTI. Similarly, the Wide Field Planetary Camera 2 (WFPC2) instrument spent 16 years on-orbit. By the time it was decommissioned, its truly severe CTI created trailing that was readily visible on every exposure.

Different astronomical measurements are hindered by different species of charge traps. Charge traps with a characteristic release time of a few CCD clock cycles move electrons by a few pixels, creating short trails that alter the apparent position (astrometry) and shape (morphology) of faint objects. Charge traps with a

*E-mail: rm@roe.ac.uk

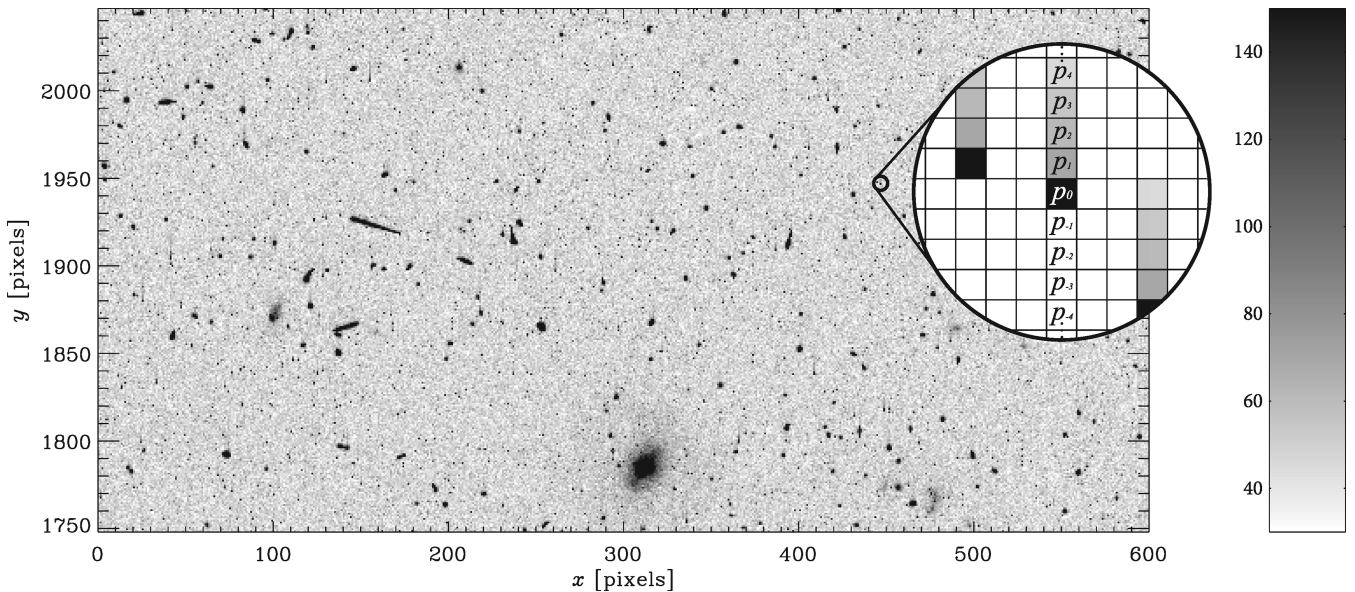


Figure 1. A typical, raw *HST* ACS/WFC image, in units of electrons. This 30×15 arcsec² (600×300 pixels) region is at the far side of the CCD to the readout register, which lies towards the bottom of the page. It was obtained on 2005 May 15, 1171 days after the launch of the ACS. Upon close inspection, as illustrated in the zoomed inset, the CTI trailing behind (above) objects is manifest.

release time of many clock cycles completely detach electrons from their original objects, thus also lowering their measured brightness (photometry). Several parametric schemes have been developed to estimate and thus correct all these effects at a catalogue level. Fitting formulae have been approximated, as a function of objects' detector position, date of observation and flux, for incorrect astrometry with the WFPC2 (Cawley et al. 2002), photometry with the ACS (Riess 2003), morphology with the Space Telescope Imaging Spectrograph (STIS) (Rhodes et al. 2004) and ACS (Rhodes et al. 2007), and others. Although such schemes provide first-order mean correction for a large number of objects, they are inaccurate for high-precision measurement of individual objects. For example, no account is made for the screening of faint objects by bright objects slightly closer to the readout register (which pre-fill charge traps) or, with extended sources, for the dependence upon object size, radial profile and shape (see discussion in Riess 2000 and Rhodes et al., in preparation).

More precise removal of CTI trailing requires manipulation of the raw pixel data, using software to move electrons back to their original locations. Since CCD readout is the last stage of data acquisition, this should be the first stage of a final data reduction pipeline (e.g. CALACS; Pavlovsky et al. 2006). Even this will never achieve precision at the level of single electrons, since charge trapping and release are stochastic, quantum mechanical effects. However, such software has been demonstrated to be much more accurate than parametric solutions for the correction of the *HST* STIS imaging (Bristow 2003a; Piatek et al. 2005, 2006, 2007) and spectroscopy (Bristow 2003b), and *Chandra* Advanced X-ray Astrophysics Facility (AXAF) Charge Coupled Device (CCD) Imaging Spectrometer (ACIS) spectroscopy (Grant et al. 2004). This approach can also provide physically motivated model parameters, rather than an ad hoc fitting function to arbitrary parameters.

In this paper, we develop an empirical but physically motivated, pixel-based CTI correction scheme for the ACS/Wide Field Channel (WFC) imaging. We concentrate on traps with release times of a few CCD clock cycles, but our algorithm is sufficiently general to

be able to incorporate additional species of traps with longer release times if necessary. In Section 2, we build a model of the readout process by measuring the rate at which the CCDs' potential wells are filled by electrons, and the properties of charge traps within those wells. In Section 3, we describe software to implement this readout model, and use the iterative approach of Bristow (2003a) to reverse the process. In Section 4, we apply this to real data and obtain better measurements of galaxy photometry, astrometry and ellipticity in the *HST* COSMOS survey. In Section 5, we discuss possible improvements to our algorithm, and summarize our work.

2 MODELLING THE ACS/WFC CCDS

2.1 Data and dates

We primarily base our analysis on the ‘_RAW’ data obtained during *HST* Cycles 12 and 13 for the COSMOS survey (HST-GO-09822, P.I.: N. Scoville). These are 2368 uniform, extragalactic exposures of 507 s each (Koekemoer et al. 2007; Scoville et al. 2007). For convenience, we first split each exposure into the four quadrants readout through different amplifiers, rotating and flipping them to orient the readout in the same direction for all. We then multiply the image by the calibrated gain (which varies slightly between amplifiers) and subtract the corresponding superbias images created by Space Telescope Science Institute (STScI). This reverts the images to units of electrons, in approximately their configuration on the CCD immediately prior to readout (but note uncertainty about the imperfectly modelled injection of charge by warm pixels during readout in Section 2.2).

We have also tested our CTE correction method in a less systematic manner on imaging from Cycle 14 (HST-GO-10496, P.I.: S. Perlmutter). This extends the analysis to nearly 2007 January, when the ACS failed. While this smaller survey provided sufficient data to verify an extrapolation of our correction parameters, such non-uniform observational strategies proved less useful for tracking the gradual CTE degradation.

Our model could also be extrapolated to correct observations obtained after servicing mission 4. However, this would be a large extrapolation, and the trap density did not necessarily continue to rise at the same rate while the instrument was offline. We would therefore recommend new calibrations as soon as sufficient images become available.

2.2 Warm pixels

A detector's CTI can be measured using First Pixel Response (FPR) tests, Extended Pixel Edge Response (EPEP) tests or ^{55}Fe radiation (Janesick et al. 2001). FPR and EPEP tests involve uniformly illuminating a CCD and measuring deviations from that uniformity in the few pixels nearest the readout register and (virtual) pixels obtained by continuing to clock charge past the end of the CCD. In addition, a radioactive iron source can be used to create a series of δ -functions on the CCD, all of a fixed energy level. Deficiencies in their shape, reveal the presence of charge traps between the event and the readout electronics.

A continuous programme of FPR and EPEP monitoring has been carried out on the ACS/WFC detectors since launch (*HST* programmes 9649, 10044, 10369 and 10732; Mutchler & Sirianni 2005). Radiation testing was performed prior to launch, but is not possible on-orbit in the *HST*.

After experimenting on all three types of data acquired in a laboratory environment, we decided that the parameters needed for our model are most easily extracted from radiation tests. Although in-flight ^{55}Fe data are unavailable, cosmic ray damage has also created randomly distributed 'warm pixels' that suffice instead (Biretta & Kozhurina-Platais 2005). Warm pixels are short circuits in the CCD electrostatic potentials used to collect charge, and continuously inject spurious charge into the device. During a long exposure, warm pixels create single-pixel δ -functions. Since the rate of charge injection varies between warm pixels, these δ -functions have a range of amplitudes. In some ways, this is actually more convenient than an ^{55}Fe source.

To identify warm pixels within each image I , we locate two-dimensional local maxima, after unsharp masking to eliminate extended objects (whether they be resolved galaxies or merely a point spread function). One such warm pixel is labelled p_0 in Fig. 1, and contains $n_e = I(p_0)$ electrons. This number has been only slightly changed during readout. We measure the trail

$$T_i(n_e) \equiv I(p_i) - I(p_{-i}), \quad (1)$$

where $p_{\pm i}$ are pixels defined relative to the location of the warm pixel p_0 in Fig. 1 and i is an integer from $i = 1-9$. Note that we could have replaced pixels with negative indices by a locally determined background level. Our better scheme is robust to the accidental inclusion of any extended sources (or cosmic rays covering more than 1 pixel) in our catalogue. Although such individual artefacts have a shape, they should not have a preferred direction on average, and therefore should not bias our measurement of T_i . Indeed, we could even have intentionally measured the trailing behind extended sources. However, in practice, averaging out their intrinsic radial profile adds more noise than the extra numbers of pixels add signal.

At the very faint end of our warm pixel catalogue, which we push down to $n_e = 100$ electrons so that it only just exceeds the background level, our algorithm often finds noise peaks instead of true warm pixels. If the noise were due to photon shot noise, these pixels would be ideal for our purposes, but it is more often read noise – which is added after clocking and therefore untraced. To

prevent the dilution of our trail measurements, we discard pixels that are not flagged as warm in at least half of the exposures. In the faintest two bins, this process removes 85 and 50 per cent of the catalogue, but quickly becomes negligible for brighter pixels. True warm pixels persist through many exposures.

We avoid 'hot' pixels containing more than 76230 electrons, which is ~ 90 per cent of the full well depth. Saturated pixels bleed charge into nearby pixels on the same column, interfering with the observed shape of the CTI trail.

Note that warm pixels also inject a low level of charge into a column of pixels during readout. This is a relatively small complication: the ratio of charge in this line to that in the δ -function is equal to the ratio of the clock speed to the total exposure time. The data can be corrected along all but the worst-affected columns by subtracting superbias frames (produced from a zero-second exposure but normal readout). We subtract bias frames before anything else, since we are trying to obtain data as it was immediately before readout. However, this is a simplification because (some of) the spurious charge was also present during readout, when the CTI trails were created. A more complete CCD model might also measure the 'temperature' of each warm pixel, then incorporate a continuous injection of charge during readout. This would be most important for measurements of the density of charge trap species with long release times, whose extended trail is partly degenerate with a constant line of charge injection (as opposed to charge re-emitted from short time-scale traps for which the original source can be readily identified). Even more worryingly, there is (unexplained) temporal structure in the injection of charge to some warm pixels that is not necessarily reproduced in the superbias frames. We therefore decided to incorporate the few per cent of columns containing the warmest pixels in the CALACS bad pixel mask. This is more severe than excluding hot pixels, since the entire rest of the column is masked.

2.3 Model assumptions and parameters

To emulate the process of CCD readout, we first need to model the collection of electrons within a pixel's potential well. In theory, the expected locations of a given number of electrons can be calculated from a model of the CCD, by solving Poisson's equation within the appropriate applied potential. Hardy, Murowinski & Deen (1998) and Seabroke et al. (2008) find that, for typical CCDs, electrons are contained within a well-defined volume – outside which their density falls rapidly to zero. Adopting this result, we shall regard a given number of electrons as filling a three-dimensional (3D) pixel up to a specific height.

We then need to model the charge traps. We assume that none is filled during integration. However, following for example Grant et al. (2004) (but not Bristow 2003a), we simplify the problem of charge capture as soon as readout begins by assuming that unoccupied traps *instantly* capture any electrons in their vicinity (i.e. all traps inside the well-defined volume get filled). In reality, there is an exponential decay time needed for traps to capture an electron, but this is typically much shorter than the electron dwell time within one CCD clock cycle (Hardy, Murowinski & Deen 1998). The rapid and efficient capture of electrons, even in locations where the electron density is low, further delineates the quantifiable volume of a pixel occupied by a given number of electrons. It also means that any charge traps physically located near the bottom of a pixel (below the ambient background level) reach the steady state of being permanently occupied, even during readout. In our model,

such traps never affect an image, so we can never probe them; but then, we never need to.

Each filled trap releases its electron after a time determined by τ , the e-folding time of an exponential decay (Shockley & Read 1952; Hall 1952). If the trap is inside the volume currently occupied by electrons, it will immediately capture a new one; if it is above, the electron will be pulled down and added back to the cloud (which thus expands and may even be exposed to new charge traps). We concentrate on species of traps with capture times τ of a few CCD clock cycles (3212 μs in the parallel direction; Sirianni et al. 2004). Traps with long release times affect the leading edge of the first bright object in a CCD column, but then reach a full steady state (at least while the rest of the object passes by) and only minimally affect its photometry, astrometry and morphology (Rhodes et al., in preparation). For a fixed clock speed, τ can be conveniently expressed in units of the number of pixels that have passed since capture.

If the charge traps are evenly distributed, we need to measure only the mean density of each species.¹ In Section 2.5, we indeed find the distribution of traps to be uniform in the y direction; we have no reason to suggest that the distribution is not similarly uniform in the other directions. In addition, our approach will internally parametrize out any smooth density gradients in the vertical direction.

We assume that each charge trap always captures a single electron. Real traps might be able to hold several, or occasionally capture none. If they hold several, and especially if the trap densities are low, simultaneous release of many electrons could produce correlated spikes in the trails. Trapping mechanisms are not yet sufficiently understood to know whether electrons are released singly or in groups (Bebek, private communication). We therefore simply assume that any multiple (or partial) occupancy of traps is equivalently modelled by an *effective* density of single-electron traps.

Finally, we ignore CCDs' three-phase clocking cycle, by which a cloud of electrons is transferred from 1 pixel to the next (Janesick et al. 2001). The transition period exposes the electron cloud to additional regions of silicon and additional charge traps. However, with our assumption of instantaneous charge capture, extra charge traps in regions between pixels can again be modelled to first order as an increase in the *effective* trap density. These traps are a fraction of a pixel nearer to (or further from) the readout register, but horizontal translations of the exponential release curve are also degenerate with a change in normalization. The only remaining finessse is that the width (and therefore the height) of the electron cloud changes during the three-phase clocking cycle, making the cloud dwell temporarily at different heights within the silicon and therefore being exposed to a different number of charge traps. We ignore this second-order effect, but incorporating a model of the full, three-phase clock cycle might be a useful exercise for future work.

Our model features the following free parameters:

- (i) number of (relevant) species of charge trap,
- (ii) characteristic release time of each species of charge trap,
- (iii) density of each species of charge trap

(or a functional form for their distribution if they are not uniformly located throughout the CCD), plus the

¹This may not be acceptable for radiation-hardened detectors in future spacecraft that suffer very few traps (see Dawson et al. 2008). In that regime, techniques like pocket pumping would be ideally suited to measuring the locations of individual traps.

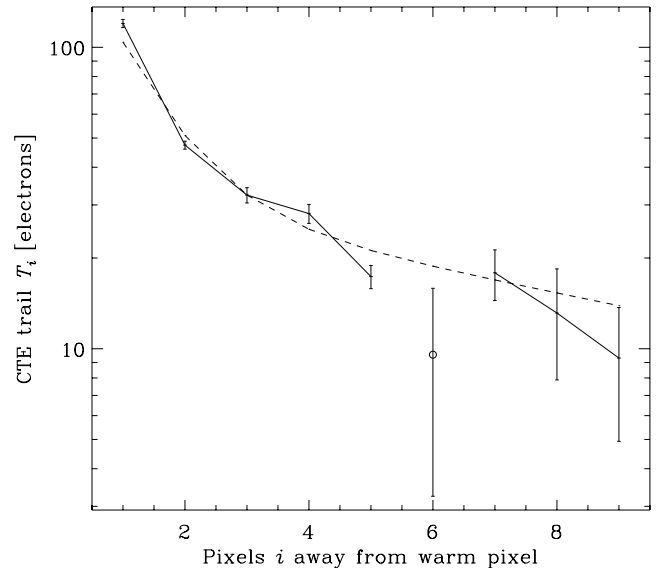


Figure 2. The mean CTI trail behind 63 901 warm pixels containing between 3234 and 76 230 electrons each, from 20 exposures obtained 1171 days after the launch of the ACS. Error bars show the 1σ scatter from measurements behind the whole population of warm pixels. The dashed curve shows the best-fitting double exponential model.

(iv) height occupied by a cloud of electrons in a pixel's potential well (i.e. the number of charge traps they are exposed to), as a function of the number of electrons.

As we shall now demonstrate, warm pixels enable us to measure all of these quantities from on-orbit science exposures.

2.4 The characteristic release times of different species of charge trap

To obtain maximum signal-to-noise ratio (S/N), we begin by studying the brightest warm pixels, furthest from the readout register and in data obtained near the chronological end of the COSMOS survey. We select 20 images taken on 2005 May 15, 1171 days after the launch of the ACS, and measure the mean trail T_i around all warm pixels between 1634 and 2039 pixels from the readout register, and containing between 3234 and 76230 electrons.² The mean trail is shown in Fig. 2.

Using Levenberg–Marquardt least-squares minimization, we find that the mean trail is well fit by a sum of two exponentials,

$$T_i = A_1 e^{-i/\tau_1} + A_2 e^{-i/\tau_2}, \quad (2)$$

where $A_1 = 327 \pm 6 e^-$, $\tau_1 = 10.4 \pm 3.2$ pixels, $A_2 = 108 \pm 3 e^-$ and $\tau_2 = 0.88 \pm 0.2$ pixels. At the -83°C operating temperature of the ACS/WFC, these correspond precisely with the release times of trap species found by Hopkinson (2001) in a Marconi CCD47-20 n-channel detector at 0.34 and 0.31 eV below the conduction band. The origin of these particular traps is unknown, but they have been speculated to be E-centres (phosphorous–vacancy complexes) with impurities of either carbon (Hopkinson 1991) or hydrogen (Tokuda & Ito 2000). Pure E-centre charge traps at 0.44 eV exist in both the Marconi and ACS/WFC (Jones 2000) CCDs, with a characteristic release time of $\tau_E \sim 300$ pixels in the Marconi. All other charge

²These values are chosen so that more bins can be added later, equally spaced in distance from the readout register and $\log(n_e)$.

traps in the Marconi CCD have $\tau < 0.01$ pixels (Hopkinson 2001), so this one-to-one correspondence is unlikely to be coincidence.

However, allowing a third exponential prevents our fit from converging, with positive A_3 but τ_3 iterating towards infinity. Fitting slowly decaying exponentials is a standard problem (e.g. Cover 2008), because they are nearly degenerate with a constant. A line of charge above a warm pixel could represent either a species of trap with a very long release time or contamination from continued charge injection during readout (cf. Section 2.3). We therefore restrict our analysis to the two species of traps with shorter τ , which also have a much more profound effect on object astrometry and morphology (Rhodes et al., in preparation). Henceforth, we shall fix the release times of the charge trap species at $\tau_1 \equiv 10.4$ and $\tau_2 \equiv 0.88$ pixels, and also fix their relative densities to be 3.0:1.³ Fitting to earlier ACS data yields consistent (but noisier) values of τ and the relative density.

2.5 Height of pixel occupied by electrons and the density of charge traps

The total number of electrons that have been displaced from a packet originally containing n_e electrons is the integral under the curve

$$\sum_1^{\infty} T_i = \frac{A_1}{e^{1/\tau_1} - 1} + \frac{A_2}{e^{1/\tau_2} - 1} (= n_q). \quad (3)$$

Since we are assuming that any traps surrounded by free electrons are instantly filled, this number of trapped electrons equals the (effective) number of charge traps n_q in the volume V traversed by electrons between their original pixel and the readout register.

The volume V is the product of the distance y to the readout register, the width of a pixel and the height within a pixel⁴ filled by n_e electrons, above a background level b . Warm pixels are available with a range of y and n_e and in images with a range of backgrounds b (this varies around $51 \pm 9 e^-$ due to the angle between the telescope and the Sun; Leauthaud et al. 2007). By counting the number of electrons trailed behind a variety of warm pixels, we directly measure $n_q(y, n_e, b)$. Note that the interpretation of electrons filling pixels to a given height is instructive but not necessary: this function is precisely what we require.

Fig. 3 shows the mean CTI trail behind warm pixels at varying distances from the readout register and of varying warmth. The top-right panel reproduces Fig. 2. The other panels show trails behind different pixels within the same set of 20 images. Although a busy plot, it has been simplified for illustration. For the real analysis, the number of bins was doubled in both y and n_e directions, and an additional dimension, with five bins of varying background level, has been marginalized over here. Towards the left-hand side, the trails may be systematically underestimated due to the inclusion in our catalogue of read noise peaks. However, the efforts in Section 2.2 to exclude them have kept this small, as demonstrated by the still-recovered shape of the trails. Each trail is fitted with double exponential decays (2), the integral under which gives the total number of trapped electrons, and hence the number of exposed traps n_q .

³ There is no reason why we would expect this to be an integer.

⁴ This assumes that the height of an electron cloud changes by only a small amount during readout; for further discussion, see Rhodes et al. (in preparation).

Fig. 4 shows the total number of charge traps exposed to each set of warm pixels for which a panel was allocated in Fig. 3. Solid lines join the data points measured at constant distances from the readout register (rows in Fig. 3). These data are well modelled by

$$\begin{aligned} n_q &= \rho_q V \\ &= \rho_q \left[\left(\frac{\max\{n_e - d, 0\}}{w} \right)^\alpha - \left(\frac{\max\{b - d, 0\}}{w} \right)^\alpha \right] y^\beta, \end{aligned} \quad (4)$$

where α , β , d and ρ_q are to be measured. Parameter w is the full well depth, which we assume to be fixed at $84\,700 e^-$ even though it varies by a few thousand electrons across the device (Gilliland 2004), and d is the depth of the supplementary buried channel or ‘notch’ in the CCDs, which we fit. The notch is a small region at the bottom of a potential well used to gather electrons when only a small number are present, much like a narrow channel cut into the bed of a water drainage canal. In our model, the notch has zero volume, so it merely adjusts the starting point of the power-law increase in height governed by α .

We again use Levenberg–Marquardt least-squares minimization to fit the free parameters. We find that $\beta = 1.01 \pm 0.01$, consistent with a uniformly increasing number of traps with increasing distance from the readout register. Since we would expect this behaviour, we explicitly fix $\beta \equiv 1$ and then obtain best-fitting values of $\alpha = 0.576 \pm 0.013$, $d = 96.5 \pm 2.0 e^-$ and $\rho_q = 0.544 \pm 0.008 \text{ pixel}^{-1}$, split between the two species of charge trap in a ratio of 3.0:1. Note that these errors do not include the uncertainty propagated from the measurement of the charge trap release times and density ratio.

2.6 Growth rate of charge traps

The ACS was installed on 2002 March 7, and cumulative radiation damage since then has gradually created more charge traps. We can use the COSMOS data, which was acquired uniformly over a long period, to track CTI degradation. Assuming that charge trap release times and the relative densities of the two species remain unchanged, we use the warmest pixels furthest from the readout register (as in Section 2.4) to measure the density of charge traps ρ_q at 12 additional times during the survey.

Fig. 5 shows the measured increase in charge trap density over time. This is fit by a constant accumulation of $(4.34 \pm 0.13) \times 10^{-4}$ traps per pixel per day, and an initial density on launch of $\rho_q^0 = 0.037 \pm 0.001$ traps per pixel (although the formal error on the latter is probably an underestimate, since the extrapolated value is very sensitive to errors in the gradient). We also tried fitting a sawtooth model in which a fraction of the traps were removed during their first subsequent anneal (as described by Cox & Cottingham (2001), the temperature is raised to 13°C about once a month; the exact dates during Cycles 12 and 13 are recorded in the Appendix). Riess (2002) and Sirianni et al. (2004) confirmed that this successfully reduces the density of hot pixels. However, the fraction of removed charge traps iterated to zero during our fit: recovering a linear model (consistent with Mutchler & Sirianni 2005) and suggesting that the anneals did not significantly improve CTE. Indeed, while hot pixels and charge traps both are likely a product of the same non-ionizing energy loss and should accumulate at the same rate, Robbins (2000) find that traps are only effectively removed by annealing at temperatures above 150°C for E-centre traps and 330°C for divacancy traps.

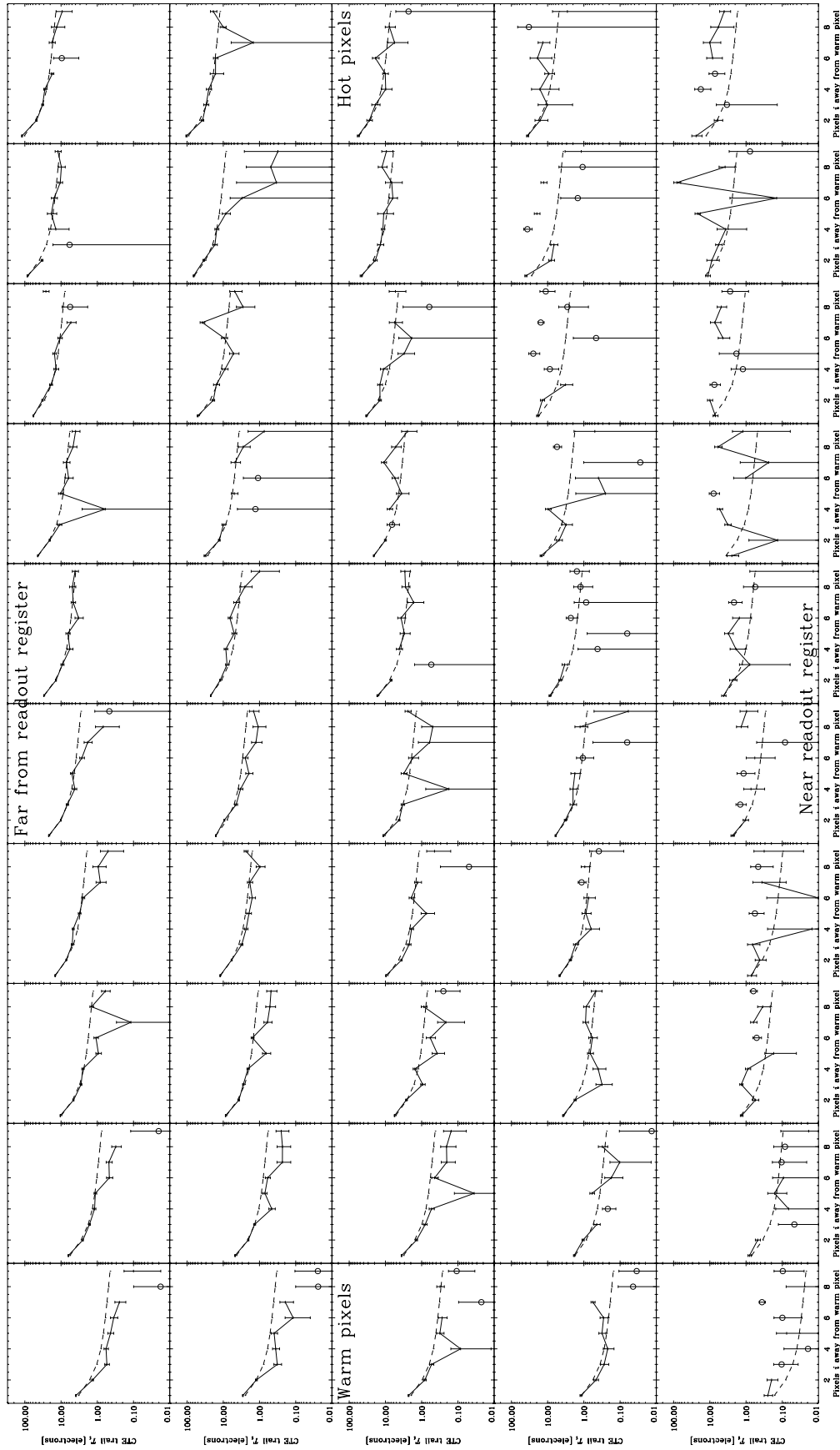


Figure 3. CTI trails behind a range of warm pixels, containing different amounts of flux (increasing left to right) and at greater distances from the readout register (increasing bottom to top). Fig. 2 is reproduced exactly in the top-right panel. The smooth dotted lines show fits of double exponential function 2, assuming a fixed ratio of the densities of different species of charge trap, and hence the same shaped curve in each case. Open circles depict negative values. These measurements can be used to probe the distribution of charge traps on the CCD, and the rate at which a pixel’s potential well fills up as a function of the incident flux, thereby exposing electrons to additional traps. The mean distances from the readout register for each row, and the flux levels for each column, are provided in Fig. 4.

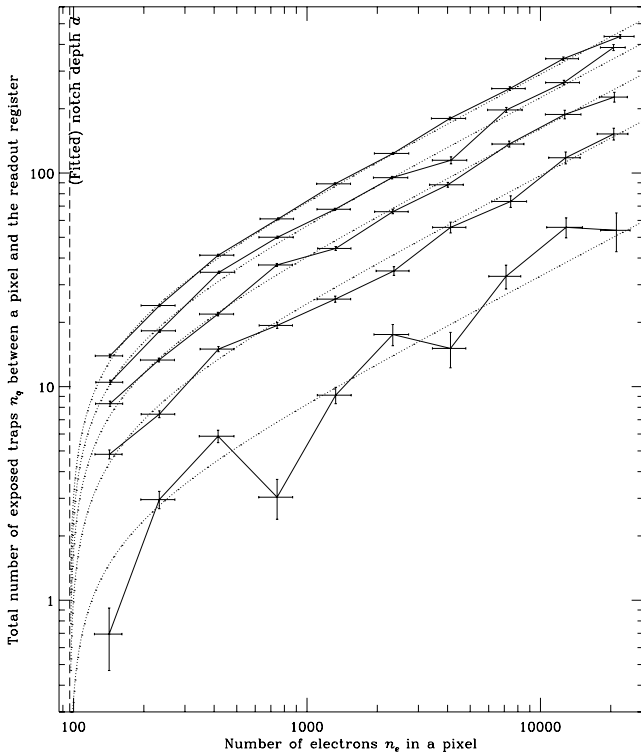


Figure 4. The total number of charge traps n_q exposed between a warm pixel and the readout register, as a function of the number of electrons n_e in that pixel. If traps are uniformly distributed, this is proportional to the height within a pixel filled by n_e electrons. Error bars are underestimated, because they do not include contributions propagated from uncertainty in τ . The solid lines join data from warm pixels 212, 618, 1024, 1430 and 1836 ± 203 pixels from the readout register (bottom to top). The cumulative number of traps increases linearly with that distance, implying that the traps are uniformly distributed throughout the CCD. The dashed curves show a model in which the electrons occupy zero volume within the CCD notch (the depth of which is a free parameter), and increase as a power law of the number of electrons above it.

3 CCD READOUT SOFTWARE

3.1 Forward operation

We now describe a software imitation of the hardware CCD readout, using the model developed in Section 2. Just like the real version on the *HST*, our software uses a fairly simple algorithm to shuffle charge to an adjacent pixel, and this is repeated many times to complete a full readout. For convenience, our code has a user interface written in IDL, but for speed the core is written in JAVA. Even so, the software algorithm is much slower than an on-board hardware readout, taking 25 min per 4096×4096 ACS/WFC image on a single 2 GHz processor, compared to 2.5 min on the *HST* (Pavlovsky et al. 2006). However, it is trivially parallelizable for multiple exposures, and need ever be run only once on any given exposure.

Since the mean density of charge traps ρ_q is known, but their exact locations are not, traps are scattered at random 3D locations within the model silicon wafer. Importantly, each trap is allocated a particular vertical height in some detector pixel. The occupancy of each will be continuously monitored. Electrons are then added into the pixel array, in the numbers we think they were at the end of an exposure.

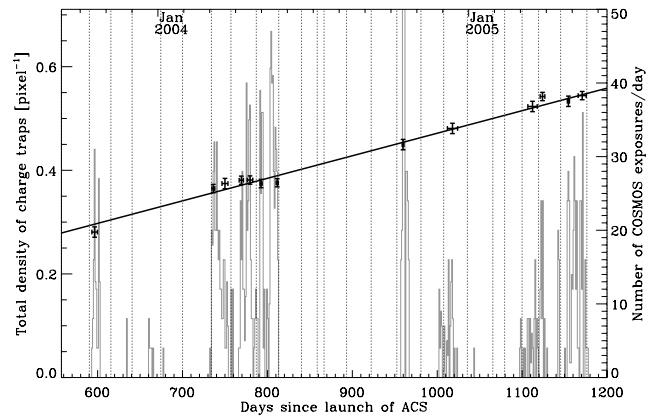


Figure 5. The accumulation of charge traps in the ACS/WFC CCDs between 2003 September 9 and the end of 2005. The data points and left-hand axis show measurements of the total density of charge traps, split between the two species in a ratio of approximately 3.0:1. Horizontal error bars show the total time during which it was necessary to average data to obtain sufficient S/N. The histogram and right-hand axis show the number of exposures taken as part of the COSMOS survey, which we analysed to obtain these figures. The dotted vertical lines show the times when the ACS CCDs were annealed (these are also listed in Table A1).

A cloud of n_e electrons is assumed to fill a pixel to a fractional height $(\max\{n_e - d, 0\}/w)^\alpha$. Any charge traps inside the occupied volume immediately capture one electron. All free electrons are then transferred instantaneously to their adjacent pixel (or to the serial register for the last pixel in parallel array, or to the pre-amplifier from the last pixel of the serial register). As discussed in Section 2, we do not attempt to model the three-phase clock cycle of a real CCD. Finally, electrons inside traps are allowed to decay with probability $1 - e^{-1/\tau}$. Released electrons are returned to the free electron pool, and the process is repeated.

Shot noise in this model created ragged trails behind faint objects and amplified background noise fluctuations. We introduce two numerical schemes to ameliorate this. First, to counter the random release or non-release of electrons from charge traps, our model traps are allowed to contain fractional numbers of electrons. In this scheme, each electron is gradually released in a floating-point exponential trail, until the trap is refilled to a whole electron by the passing of a new bright pixel (removing only a fractional number of electrons from the free pool). After readout, the number of electrons in each pixel is rounded back to an integer value for storage. Secondly, to counter the necessarily random locations of model traps, we can run the code multiple times with different random seeds and average the results. To save CPU time, this is equivalently implemented by increasing the density of traps by a factor of 3 (or any other number specified as an optional input parameter), each of which is only allowed to contain a third of an electron. This most improves the sampling of traps in the thin slice of the CCD above the image background level that profoundly affect faint sources. With both schemes, the change in background noise level during readout becomes less than 1 per cent.

3.2 Reverse operation

Moving electrons back to where they belong, and thus removing the CTI trails, requires the image mapping to be inverted. This is not analytically possible. However, the trailing represents a small perturbation around the true image, so it can be achieved using the forward algorithm, via an iterative approach. Following Bristow

Table 1. Iterative method to remove CTI trailing, using only a forward algorithm that *adds* trailing. The true image I is desired but not available. Only a version with (a small amount of) trailing, $I + \delta$, can be obtained from the telescope. However, by running that image through a software version of the readout process, and subtracting the difference, deviations from the true image can be reduced to $\mathcal{O}(\delta^2)$. Successive iterations further reduce the trails until an image is produced that, when ‘readout’, reproduces data arbitrarily close to those obtained from the telescope. This is the corrected image.

True image	I Not available	
Downloaded from <i>HST</i>	$I + \delta$	(A)
After one extra readout	$I + 2\delta + \delta^2$	(B)
(A)+(A)–(B)	$I - \delta^2$	(C)
After another readout	$I + \delta - \delta^2 - \delta^3$	(D)
(A)+(C)–(D)	$I + \delta^3$	(E)
After another readout	$I + \delta + \delta^3 + \delta^4$	(F)
(A)+(E)–(F)	$I - \delta^4$	etc.

& Alexov (2002), Bristow (2003a) and Bristow, Kerber & Rosa (2005), Table 1 describes a way to obtain an image that, after a software readout, reproduces the data actually downloaded from the *HST*. This is the desired, corrected image. Images (A), (C), (E), etc., can all be obtained and, after several iterations, converge to that ideal.

In practice, excellent results are obtained after only a single iteration. Indeed, since the CCD filling and readout models are unlikely to match the real hardware better than $\mathcal{O}(\delta^3)$, only the first iteration is even useful. To speed the correction of the 2368 COSMOS exposures, we therefore restricted our correction of the larger data set to a single iteration. Fig. 6 shows the image from Fig. 1 after correction, using one iteration.

3.3 Additional features of the software

Our CCD readout software has several additional features that we did not find necessary for CTI correction in ACS/WFC, but which may be useful for other instruments. We document these features here for completeness and future reference.

Although we used only two species of charge trap, the code is capable of handling many (currently up to four) different species, each with a density ρ_q and characteristic release time τ . With additional measurements of flux loss due to long-lifetime charge traps, this could be used to more accurately correct photometric measurements of astronomical sources.

The code can shuffle electrons both in the parallel direction and along a serial register. In this mode, the execution time is doubled. Charge traps in the serial register, with characteristic release times similar to the serial clock speed, can create trails at 90° to those described by 1. However, it is well established (e.g. Riess 2003; Mutchler & Sirianni 2005) that the serial CTE in the ACS/WFC CCDs is very high, and that trailing is almost exclusively in the parallel direction. Indeed, we attempted to measure serial CTI trails but found a signal consistent with zero. We therefore neglected this entire mechanism.

By default, the code places model charge traps randomly within the model CCD. These are not at the same locations as the charge traps in the real CCD, which introduces additional noise during the correction. This is ameliorated by increasing the density of traps but decreasing their capacity as described in Section 3.1. However, radiation-hardened detectors in future cameras (e.g. Dawson et al.

2008) may contain sufficiently few traps for this noise to become significant. If their individual locations could be measured on-orbit, for example via pocket pumping, the code can place model traps at the correct locations.

4 TESTING THE CORRECTION

4.1 Warm pixel trails

Fig. 7 shows the residual CTI trails measured from corrected versions of the images used for Fig. 3. Note the reduction in the level of all trails by a factor of about 30. This reduction is matched or bettered during all four times (the first, sixth, seventh and thirteenth data points in Fig. 5) when many COSMOS exposures happened to be obtained during a single day, and a more precise measurement could be made. This demonstrates that we have achieved an approximately $(1 - 1/30) = 97$ per cent precision in our trapping and readout model, at all locations on the CCD array and for traps at all heights within the CCD.

If the images are instead corrected using two iterations of the method in Table 1, the data points in Fig. 7 move only within their error bars, justifying our use of only one iteration for the sake of speed.

4.2 Galaxy photometry measurement

We now stack the corrected images to create 577 ‘_sci’ science frames, following the pipeline of Koekemoer et al. (2007), which makes use of the DRIZZLE/MULTIDRIZZLE software (Fruchter & Hook 2002; Koekemoer et al. 2002). There are four exposures per pointing, dithered almost along a straight line (two exposures separated by 6.1 arcsec at an angle of 91.2° from the coordinate frame and another pair, separated by 3.1 arcsec from the first, at an angle of 85.4°). These are transformed into a projection of the pixel array on to the sky, with oversampled 0.03 arcsec pixels that are aligned with the instrument coordinate frame to keep the two readout registers at the top and bottom. The dithers complicate the issue of how far each galaxy is from the readout register, because it was in different areas of the focal plane in different exposures. To roughly divide the catalogue into objects at final positions (x, y) that have traversed different numbers of charge traps, we calculate

$$n_{\text{transfers}} = \max\{0, 2048 - |6046 - 1.67y - 0.0614x|\} \quad (5)$$

and separately consider objects with values of $n_{\text{transfers}}$ in the ranges 0–475, 475–950, 950–1425, 1435–1900 and 1900–2048. The final bin also includes most of the area of the oversampled images in which only data were available from only three of the four exposures, due to the gap between the CCDs.

Fig. 8 shows the changes to galaxy photometry during CTE correction, as measured on the original versus corrected images by the *Source Extractor* (Bertin & Arnouts 1996). As expected from Riess (2003), we find that the most affected sources are faint galaxies far from the readout register. The amount of change is in line with the extrapolated prediction of Riess & Mack (2004). Note however that *this should not be interpreted as the error in point-source photometry on uncorrected images*. In particular, our correction scheme does not currently include any species of charge traps with very long release times, which may steal additional flux from sources. Our resolved sources also contain additional electrons in extended wings that, according to our well filling model, lie near the bottom of the pixel potential, occupy a relatively large volume of silicon and are exposed to a greater number of charge traps.

Photometric measurements can also be expressed in terms of the galaxies' detection S/N. The interpretation for galaxies with $S/N < 20$ is complicated by two issues. First, a selection bias in which sources whose detection S/N increased greatly were not included in the pre-correction catalogue. Secondly, the correction is a form of unsharp masking, and noise in adjacent pixels becomes less correlated during correction. As discussed in Rhodes et al. (in preparation), this can actually lower the detection S/N of faint sources.

4.3 Galaxy astrometry measurement

The change in galaxies' positions during CTI correction is shown in Fig. 9. The spurious shift is $2.42 \pm 0.17 \times 10^{-6}$ arcsec per (0.05 arcsec) pixel transfer for galaxies between magnitudes 17 and 19, and 0.57 ± 0.24 arcsec per transfer for 25 th to 27 th magnitude galaxies.

The distance depends as expected upon distance from the read-out register, but is initially surprising as a function of galaxy flux. Using very similar code, Bristow (2004) found bright point sources

to be less affected than faint ones. Our own code also moves a given object less if its flux is increased. However, bright resolved sources also tend to be larger than faint ones. Astrometry is most affected by charge traps with short release times (Rhodes et al., in preparation), which are now able to capture, move and release an electron several times within a large galaxy. Furthermore, the non-linear well-filling model ensures that even electrons in the low-level, extended wings are exposed to most of the charge traps seen by the core. Multiple trapping does not remove flux from a galaxy, so should not impact photometric measurements. However, this process breaks the standard argument whereby charge traps saturate, with empty traps being newly exposed only by relatively large increases in flux. Subtle effects like this highlight the power of a pixel-based method: they are unlikely to be matched in a parametric scheme acting at a catalogue level.

4.4 Galaxy shape measurement

Fig. 10 shows the change in galaxies' full width at half-maximum (FWHM) size during CTI correction, as measured by the *Source*

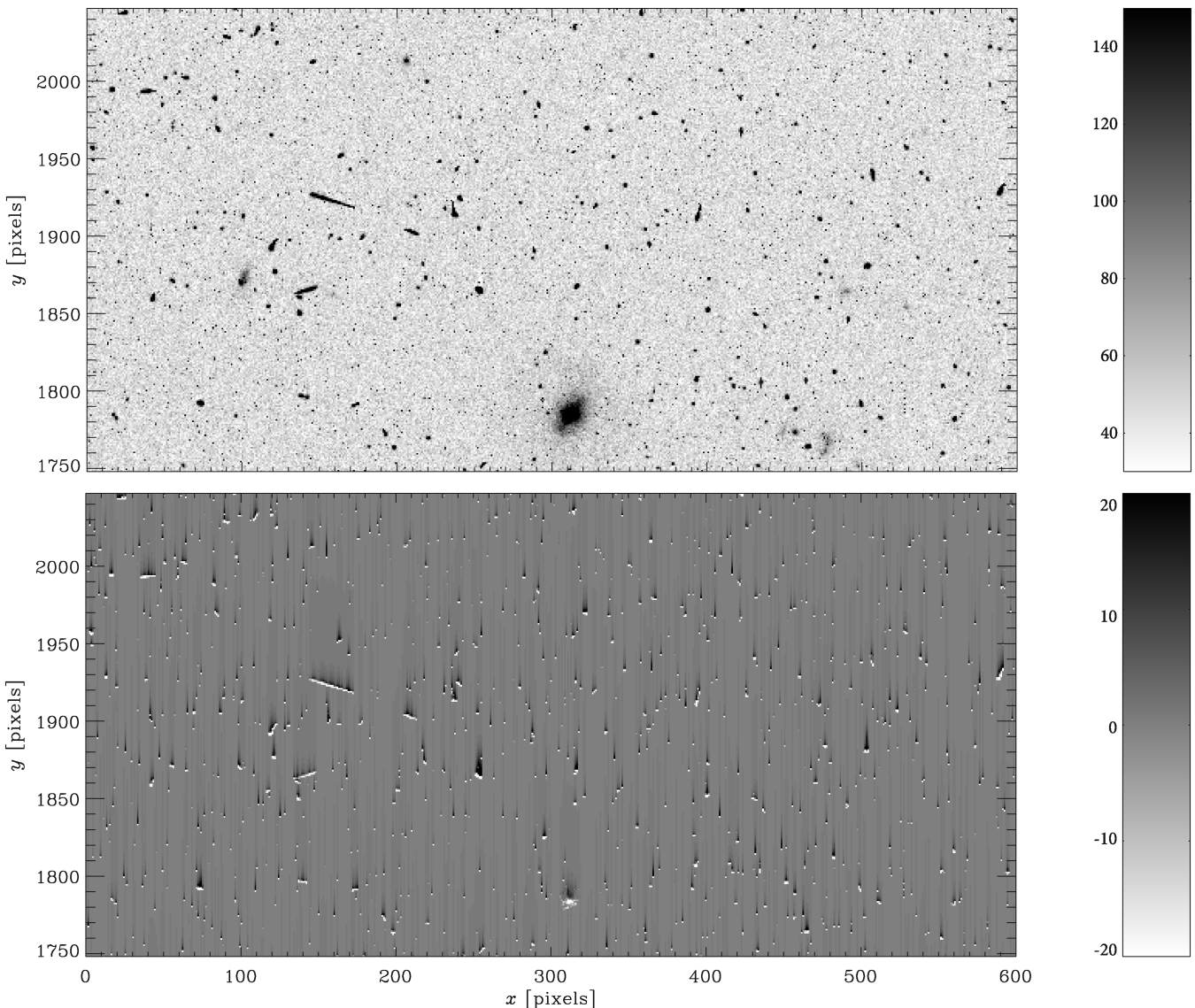


Figure 6. Top panel: the *HST* ACS/WFC image from Fig. 1, after CTI correction, in units of electrons. Bottom panel: difference image.

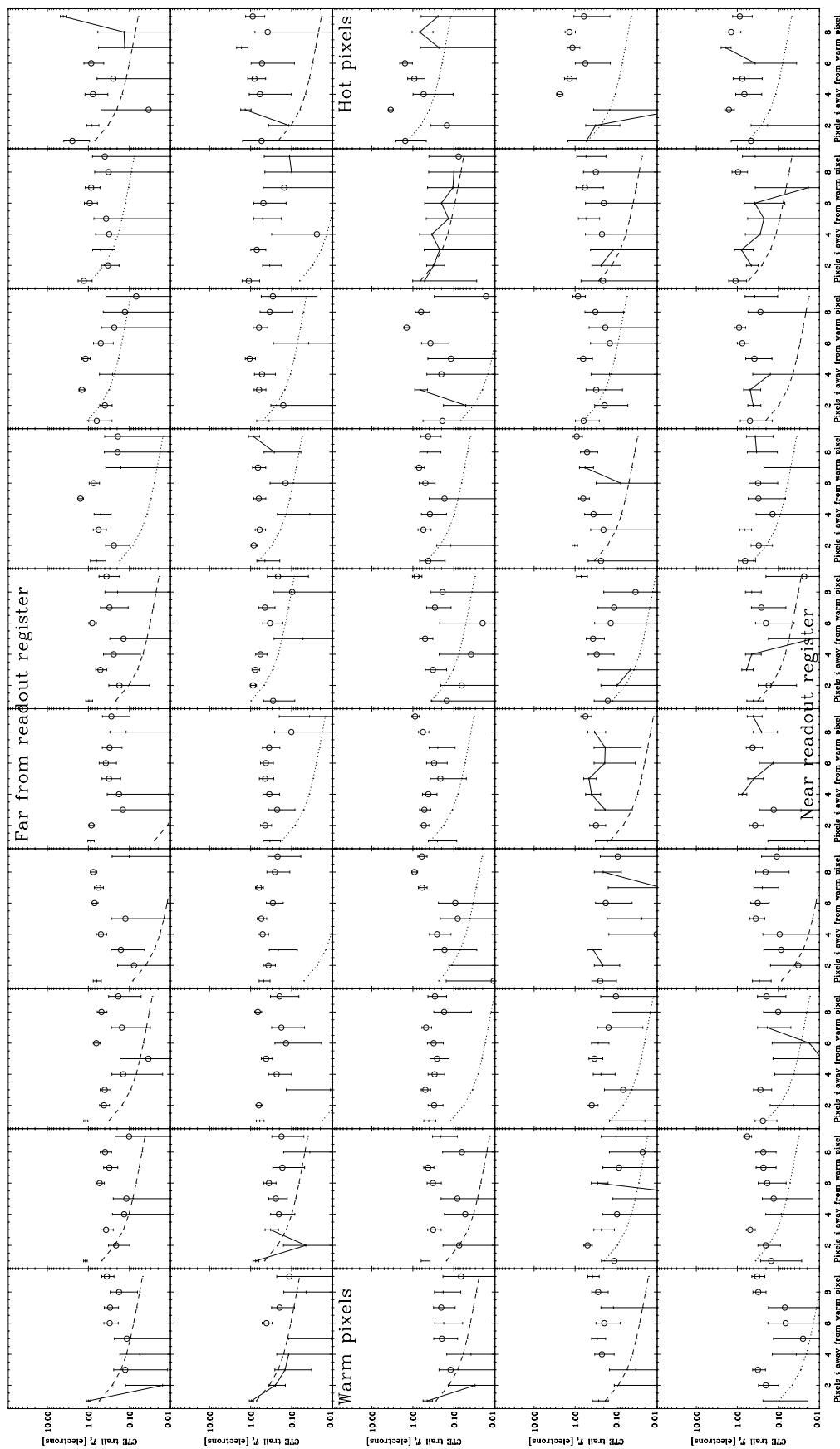


Figure 7. Measurement of the CTI trails from the same images used in Fig. 3, after correction. The y-axes are logarithmic; open circles and dotted (rather than dashed) lines show negative values.

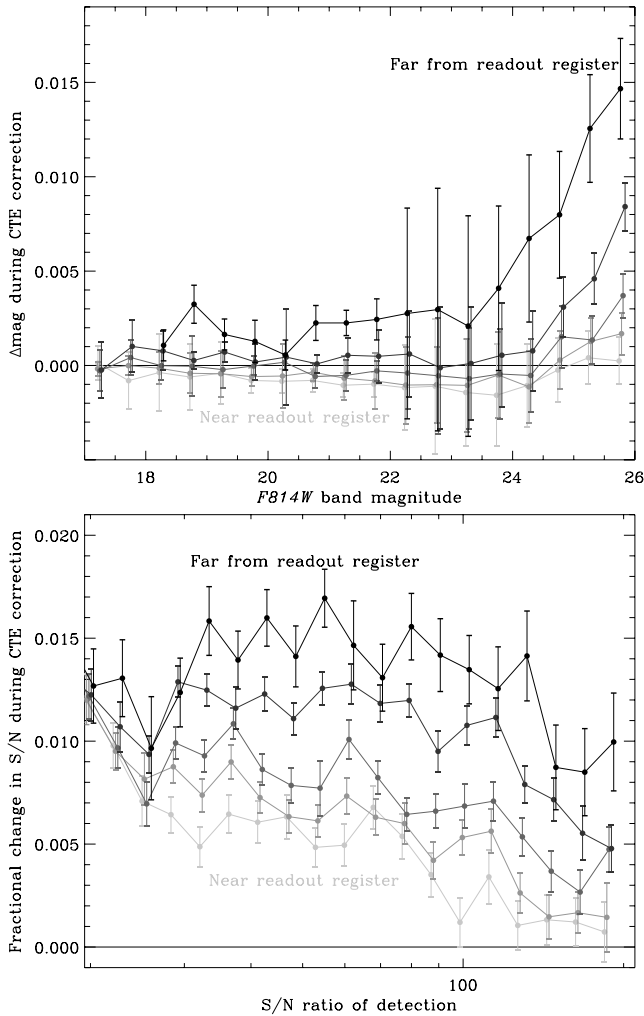


Figure 8. Changes in galaxy photometry during CTI correction, as a function of the measured magnitude and detection S/N in the corrected images. A fractional change is calculated as $(\text{old} - \text{new})/\text{new}$. The five lines connect subsets of galaxies between approximately 0–475, 475–950, 950–1425, 1435–1900 and 1900–2048 transfers from the readout register; the photometry is measured on stacked exposures and the exact number of transfers varies slightly between dithers. The points show the median value in the top panel, since the distribution of points is highly skewed, and the mean value in the bottom panel, which is less so. Error bars show 68 per cent confidence limits on the mean.

Extractor (Bertin & Arnouts 1996). The CTI trails had spuriously enlarged objects, which are shrunk slightly when the flux in the trails is pushed back into the core. The effect increases as expected with the number of charge transfers, and is most pronounced in faint galaxies, which are intrinsically smallest, and also encounter the largest number of charge traps per electron during readout.

Galaxy ellipticities are a particularly interesting case because the *true* value of ellipticity is known, at least statistically. If there is no preferred direction in the Universe, galaxies cannot preferentially align in any direction and their mean ellipticity ought to be zero. However, the CTI trails coherently elongate galaxies in the readout direction.

In practice, high-precision measurements of galaxy shapes are made difficult because they are imprinted with the shape of the tele-

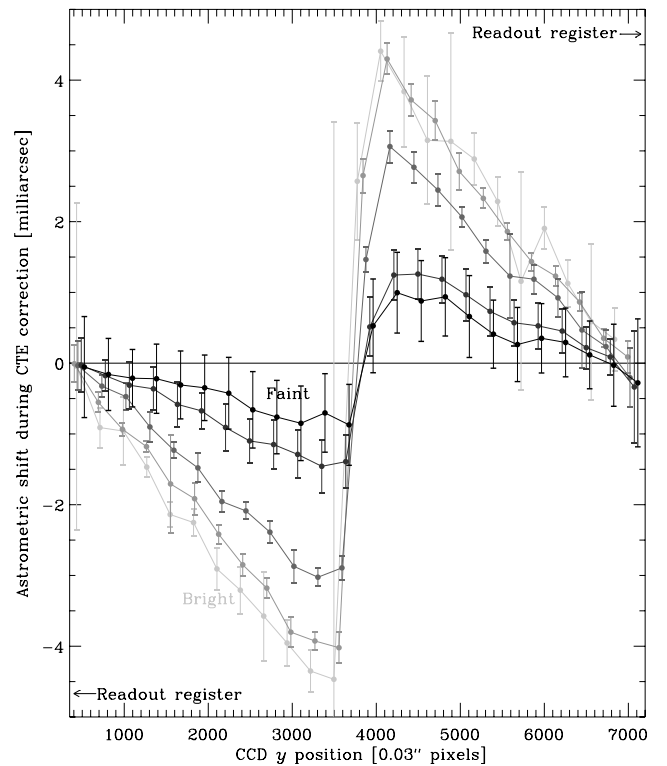


Figure 9. Change in galaxy astrometry during CTI correction, in the direction of the readout registers. Readout registers are located at opposite edges of the array, with pixels from each half being readout at their nearest register. Solid lines connect subsamples of galaxies between magnitude limits of $F814W = 17\text{--}19$, $19\text{--}21$, $21\text{--}23$, $23\text{--}25$ and $25\text{--}27$. For the sake of clarity in this figure, the points show medians in each bin. The error bars show 68 per cent confidence limits, and the mean values behave consistently around these bounds, but noise renders the overall behaviour less clear. Note that faint galaxies are also typically smaller than bright galaxies, unlike the point sources used in previous studies.

scope’s PSF. Furthermore, the ACS/WFC PSF changes during orbit, as the *HST* expands or contracts due to thermal shifts. Most inconveniently, the predominant PSF patterns happen to align themselves with the readout direction and also tend to align galaxies in that direction (Rhodes et al. 2007). Fortunately, a great deal of software has been developed for effectively ‘deconvolving’ galaxy ellipticities from the PSF, in order to measure weak gravitational lensing. We use the algorithm by Rhodes, Refregier & Groth (2000), as implemented by Leauthaud et al. (2007) and Massey et al. (2007a,b), to recover the underlying galaxy ellipticities.

The top panel of Fig. 11 shows how galaxies appear spuriously elongated in the direction of the readout registers before CTE correction. The faintest galaxies are worst affected, although the elongation is also seen in the brightest galaxies. As shown in Rhodes et al. (in preparation), the effect is also worst for galaxies intrinsically elongated perpendicular to the readout direction. Neither such effect is modelled by the parametric correction of Rhodes et al. (2007). The mean spurious ellipticity of galaxies in the faintest two bins increases as approximately $(24.3 \pm 2.9) \times 10^{-6}$ per (0.05 arcsec pixel) transfer and $(7.7 \pm 2.0) \times 10^{-6}$ per transfer. The noise is predominantly due to the process of PSF deconvolution. After CTI correction, as shown in the bottom panel, this effect has been successfully reduced to $(0.2 \pm 3.1) \times 10^{-6}$ and

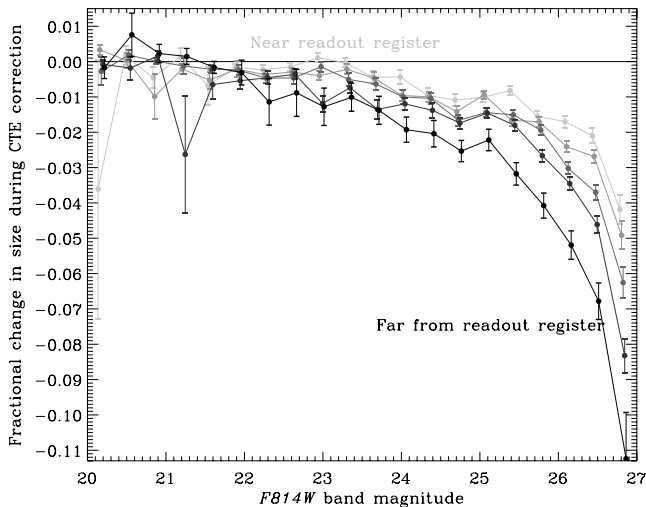


Figure 10. Change in galaxy FWHM size during CTE correction. Solid lines connect the same samples as in Fig. 8. Points show mean values within bins and 68 per cent confidence limits.

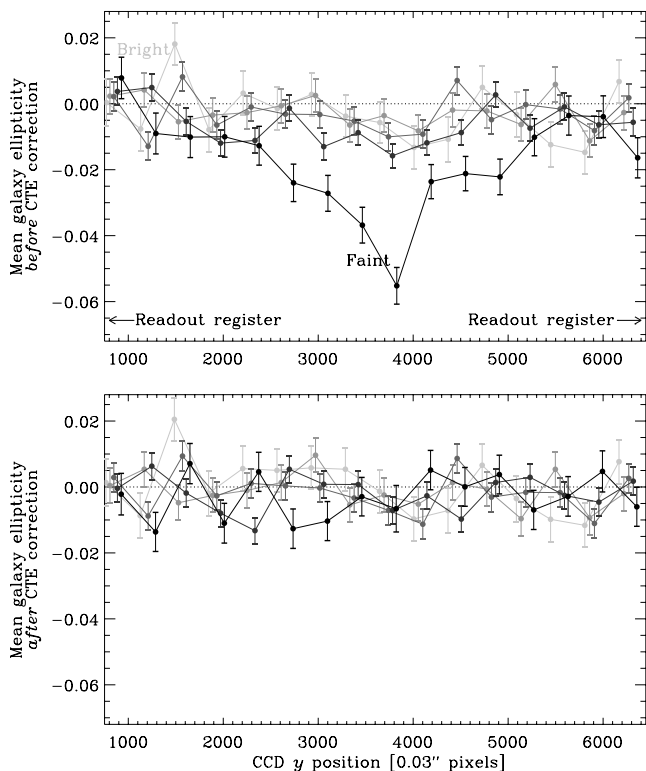


Figure 11. Component of mean galaxy ellipticities in the direction of the readout registers ($e \cos 2\theta$, where e is the ellipticity and θ is the angle between the major axis and the line joining opposite sides of the CCD) before and after CTE correction. Values are shown after correction for convolution with the PSF, whose shape is imprinted on the galaxies, but this correction increases the scatter. Solid lines connect subsamples of galaxies within magnitude limits of $F814W = 22-23$, $23-24$, $24-25$, $25-26$ and $26-27$. Points show mean values in bins and 68 per cent confidence limits.

$(2.2 \pm 2.1) \times 10^{-6}$. The mean shear is similarly reduced by an order of magnitude from (1.5 ± 0.1) to (0.2 ± 0.2) per cent in the faintest bin, and from $(7.4 \pm 1.1) \times 10^{-6}$ to $(0.9 \pm 1.1) \times 10^{-6}$ overall.

5 DISCUSSION AND CONCLUSIONS

We have corrected CTI trailing in ACS/WFC images by more than an order of magnitude. As demonstrated by the improvement of *HST* COSMOS survey images between Figs 3 and 7, and in Fig. 11, we have achieved a 90–99 per cent precision in our model, at all locations on the CCD array and for traps at all heights within the CCD. Our method works at the pixel level, moving individual electrons back to locations from which they were dragged during readout, and model parameters correspond to real, physical properties of the device. This is far better than the ad hoc, parametric correction described by Rhodes et al. (2007). Since the trails are created during the final step of data acquisition, the correction should be applied as the first step in data reduction and analysis.

As suggested by Biretta & Kozhurina-Platais (2005), warm pixels in the detectors were successfully used to measure device properties including the charge trap density and release times. The ubiquitous distribution of warm pixels allows the locations of charge traps to be continuously measured across the CCD, using in-orbit science data. Exceeding earlier expectations, however, the range of flux levels in warm pixels can also be used to obtain the 3D height of the traps, and the rate at which electrons fill up the volume of a pixel's potential well. All of these parameters are needed to correct CTI trailing, and it is remarkable that they can all be measured using a separate consequence of the radiation damage. To improve on this with future large surveys will probably require laboratory-based measurements of the CCD and charge trap characteristics before launch (and possibly after retrieval), or the integration of on-board electronics to allow in-flight tests such as pocket pumping.

We find two significant species of charge traps that affect the astrometry and morphology of astronomical objects, with characteristic release times $\tau = 10.4 \pm 3.2$ and 0.88 ± 0.2 pixels. These accumulated in a ratio of approximately 3.0:1 and, by the end of *HST* Cycle 13, there was slightly more than one in every other pixel, uniformly distributed throughout the CCD. An electron beginning 2048 pixels away from the readout register therefore encounters a large number of traps during readout. The (random) locations of traps in our model are inevitably different to those in the real CCD. This adds shot noise during correction that is particularly notable in the structure of the image background. We have eliminated half of the shot noise by increasing the density of model traps density and allowing them to hold non-integer amounts of charge.

We did not attempt to measure the density of traps with very long release times. As shown by Rhodes et al. (in preparation), these primarily affect object photometry. They can be measured using repeated images of standard stellar fields, such as the STScI internal CTE calibration programme. Alternatively, once the uniform distribution of other charge trap species has been established, they could also be measured from EPER or FPR tests. If their density is measured after servicing mission 4, our software can easily handle additional species of charge traps, and thus improve the simultaneous correction of object photometry, astrometry and morphology.

We measure a functional form describing the rate at which electrons fill up the volume of a pixel's potential well. Below a 'notch' depth of $96.5 \pm 2.0 e^-$, they occupy negligible volume; additional electrons overflow and the cloud expands with a power law of index $\alpha = 0.576 \pm 0.013$. This volume determines the number of traps

encountered by the cloud, as it is moved through the CCD substrate towards the readout register. Note that, in order to cope with the huge data volume, we developed the model stepwise: fixing the first measured parameters before fitting the later ones. Since errors on some measurements were not carried through, these later errors are likely to be underestimated.

Our pixel filling model neatly illustrates why CTI trailing is a non-linear function of object flux, and why it can be reduced by pre- or post-flashing an image to increase the background level. During readout, the large cloud of electrons within a bright source has to navigate more charge traps than the small cloud within a faint source – but the ratio of exposed traps to electrons falls as $n_q/n_e \approx n_e^{\alpha-1}$. Since $\alpha < 1$, the fractional amount of charge that gets trailed behind a faint source is greater than that behind a bright source. In addition, a fat zero reduces the *total* amount of trailing behind all sources by moving all pixels to the right in Fig. 4. For faint sources of fixed flux, the total number of exposed traps is proportional to $d n_q/d n_e$, which decreases as $\sim(b-d)^{\alpha-1}$.

The two biggest simplifications in our model are reducing the three-phase clocking cycle to a single shift, and not explicitly treating the continuous injection of charge from warm pixels during readout. The latter would be particularly important if this method were required for measurements of charge traps with long release times. Improvements in these areas would be interesting directions for future studies.

ACKNOWLEDGMENTS

The authors gratefully thank Chris Bebek, Paul Bristow, Marissa Cevallos, Nick Cross, Kyle Dawson, Andy Fruchter, Nigel Hambly, Mike Lampton, Michael Levi, Max Mutchler, Natalie Roe, George Seabroke, Suresh Seshadri, Patrick Shopbell, Tim Schrabback and Roger Smith for sharing their expertise. The *HST* ACS CTI calibration programme is funded through NASA grant HST-AR-10964. The *HST* COSMOS Treasury programme was funded through NASA grant HST-GO-09822 with P.I. Nick Scoville. RM is supported by STFC Advanced Fellowship PP/E006450/1 and FP7 grant MIRG-CT-208994. AL acknowledges support from the Chamberlain Fellowship at LBNL and from the Berkeley Center for Cosmological Physics.

This work was based on the observations with the NASA/ESA *HST*, obtained at the Space Telescope Science Institute, which is operated by AURA Inc, under NASA contract NAS 5-26555.

REFERENCES

Bertin E., Arnouts S., 1996, *A&AS*, 117, 393
 Biretta J., Kozhurina-Platais V., 2005, Instrument Science Report WFPC2-2005-001
 Bristow P., 2003a, Instrument Science Report CE-STIS-2003-001, preprint (astro-ph/0310714)

Bristow P., 2003b, Instrument Science Report CE-STIS-2003-002, preprint (astro-ph/0310710)
 Bristow P., 2004, Instrument Science Report CE-STIS-2004-003
 Bristow P., Alexov A., 2002, Instrument Science Report CE-STIS-2002-001, preprint (astro-ph/0211652)
 Bristow P., Kerber F., Rosa M., 2006, in Koekemoer A., Goudfrooij P., Dressel L., eds, Proc. HST Calibration Workshop 2005. Space Telescope Science Institute, Baltimore, MA, p. 299
 Cawley L., Goudfrooij P., Whitmore B., Stiavelli M., STScI CTE Working Group, 2002, in Cox C., Cottingham C., eds, Instrument Science Report WFC3-2001-005
 Cover K., 2008, *Rev. Sci. Instrum.*, 79, 055106
 Cox C., Cottingham C., 2001, Instrument Science Report ACS-2001-05
 Dawson K. et al., 2008, *IEEE Trans. Nuclear Sci.*, 55, 1725
 Fruchter A. S., Hook R. N., 2002, *PASP*, 114, 144
 Gilliland R., 2004, Instrument Science Report ACS-2004-01
 Grant C., Bautz M., Kissel S., LaMarr B., 2004, *SPIE*, 5501, 177
 Hall R., 1952, *Phys. Rev.*, 87, 387
 Hardy T., Murowinski R., Deen M., 1998, *IEEE Trans. Nuclear Sci.*, 45, 154
 Hopkinson G., 1991, Proton Radiation Testing of CCDs for the SILEX Programme (<https://escies.org/GetFile?rsrcid=1021>)
 Hopkinson G., 2001, *IEEE Trans. Nuclear Sci.*, 48, 6
 Janesick J., 2001, *Scientific Charge-Coupled Devices*, xvi. SPIE Optical Engineering Press, Bellingham
 Jones M., 2000, Instrument Science Report ACS-2000-09
 Koekemoer A. M., Fruchter A. S., Hook R. N., Hack W., 2002, in Arribas S., Koekemoer A. M., Whitmore B., eds, HST Calibration Workshop. STScI, Baltimore, p. 337
 Koekemoer A. et al., 2007, *ApJS*, 172, 196
 Leauthaud A. et al., 2007, *ApJS*, 172, 219
 Massey R. et al., 2007a, *ApJS*, 172, 239
 Massey R. et al., 2007b, *Nat*, 445, 286
 Mutchler M., Sirianni M., 2005, Instrument Science Report ACS-2005-003
 Pavlovsky C. et al., 2006, 'Advanced Camera for Surveys Instrument Handbook' version 7.1. STScI, Baltimore
 Piatek S. et al., 2005, *AJ*, 130, 95
 Piatek S. et al., 2006, *AJ*, 131, 144
 Piatek S. et al., 2007, *AJ*, 133, 818
 Rhodes J., Refregier A., Groth E. J., 2000, *ApJ*, 536, 79
 Rhodes J. et al., 2004, *ApJ*, 605, 29
 Rhodes J. et al., 2007, *ApJS*, 172, 203
 Riess A., 2000, Instrument Science Report WFPC2-2000-004
 Riess A., 2002, Instrument Science Report ACS-2002-09
 Riess A., 2003, Instrument Science Report ACS-2003-009
 Riess A., Mack J., 2004, Instrument Science Report ACS-2004-009
 Robbins M., 2000, The Radiation Damage Performance of Marconi CCDs, Marconi Technical Note S&C 906/424
 Scoville N. et al., 2007, *ApJS*, 172, 38
 Seabroke G. et al., 2008, *A&A*, 480, 753
 Shockley W., Read W., 1952, *Phys. Rev.*, 87, 835
 Sirianni M., Mutchler M., Clampin M., Ford H., Illingworth G., Hartig G., van Orsow D., Wheeler T., 2004, *Proc. SPIE*, Vol. 5499, p. 173
 Tokuda Y., Ito A., 2000, *Materials Sci. Eng. B*, 71, 1

APPENDIX A: CCD ANNEAL DATES**Table A1.** Dates and times when the ACS detectors were annealed during *HST* Cycles 12 and 13.

Date	Time
2003 September 9	08:34:58
2003 October 12	07:09:36
2003 November 6	15:11:06
2003 December 1	15:48:13
2004 January 4	09:01:30
2004 January 30	01:08:26
2004 March 4	01:21:04
2004 March 27	00:59:38
2004 April 25	21:31:00
2004 May 22	07:34:57
2004 June 18	04:36:37
2004 July 6	16:28:51
2004 July 14	16:52:05
2004 August 10	04:41:59
2004 September 8	06:01:41
2004 October 8	09:05:45
2004 November 5	19:42:53
2004 December 2	14:11:50
2004 December 30	12:40:00
2005 January 29	11:00:00
2005 February 12	09:04:52
2005 March 4	22:55:30
2005 March 24	09:12:24
2005 April 19	07:33:57
2005 May 20	05:00:00
2005 June 12	22:35:22
2005 July 16	07:58:20
2005 August 11	20:37:49
2005 September 9	08:45:56
2005 October 8	10:06:47
2005 November 3	15:20:00
2005 November 25	08:37:56
2005 December 31	04:30:00

This paper has been typeset from a \TeX/L\AA\TeX file prepared by the author.